



OPEN

Shaping plasmon beams via the controlled illumination of finite-size plasmonic crystals

SUBJECT AREAS:

NANOPHOTONICS AND
PLASMONICS

METAMATERIALS

OPTOELECTRONIC DEVICES AND
COMPONENTS

OPTICAL SPECTROSCOPY

J.-S. Bouillard*, P. Segovia, W. Dickson, G. A. Wurtz & A. V. Zayats

Department of Physics, King's College London, Strand, London WC2R 2LS, United Kingdom.

Received
28 July 2014Accepted
31 October 2014Published
28 November 2014

Correspondence and
requests for materials
should be addressed to
P.S.O. (paulina.
segovia_olvera@kcl.
ac.uk)

* Current address:
Department of Physics
and Mathematics,
University of Hull,
Cottingham Road,
Hull, HU6 7RX, United
Kingdom.

Plasmonic crystals provide many passive and active optical functionalities, including enhanced sensing, optical nonlinearities, light extraction from LEDs and coupling to and from subwavelength waveguides. Here we study, both experimentally and numerically, the coherent control of SPP beam excitation in finite size plasmonic crystals under focussed illumination. The correct combination of the illuminating spot size, its position relative to the plasmonic crystal, wavelength and polarisation enables the efficient shaping and directionality of SPP beam launching. We show that under strongly focussed illumination, the illuminated part of the crystal acts as an antenna, launching surface plasmon waves which are subsequently filtered by the surrounding periodic lattice. Changing the illumination conditions provides rich opportunities to engineer the SPP emission pattern. This offers an alternative technique to actively modulate and control plasmonic signals, either via micro- and nano-electromechanical switches or with electro- and all-optical beam steering which have direct implications for the development of new integrated nanophotonic devices, such as plasmonic couplers and switches and on-chip signal demultiplexing. This approach can be generalised to all kinds of surface waves, either for the coupling and discrimination of light in planar dielectric waveguides or the generation and control of non-diffractive SPP beams.

The coherent control of optical waves by shaping the phase and amplitude of interfering wavefronts has recently resulted in significant progress in non-diffracting optical and surface plasmon polariton (SPP) beam^{1–3} routing, directional coupling, optical signal switching^{4–6} and flat lenses^{7,8} as well as new types of holograms^{9,10}. SPP waves, important for applications in sensing, nonlinear optics and optical interconnect applications, are uniquely positioned to take advantage of a coherent control approach as in many cases, one type of nanostructures or another, e.g., particles, grooves, plasmonic crystals, are used to couple optical signals to SPP waves and control the SPP propagation direction^{11–14}. Thus, the phase of the SPP beams can be designed at the point where controlled coupling of optical beams to SPPs takes place. Further adjusting the position of additional scatterers to modify both the direction and phase during SPP-in-SPP scattering, provides the freedom of design required to achieve phase and amplitude control. This has been used to achieve efficient launchers for SPPs and, in particular, finite-size SPP beams (including non-diffracting SPPs) by controlling the separation between and width of the grooves as well as building more complex optical antennas^{2,3,15–17}. Unidirectional, wavelength-selective and broadband photon-to-SPP and SPP-to-photon scattering have been demonstrated using this approach^{16,18–20}.

SPP crystals (SPPCs) — metal surfaces periodically structured on the SPP wavelength scale — have gained increasing attention due to their ability to control SPP generation and propagation through easily geometrically adjustable parameters such as the period or primitive cell geometry of the crystal. In analogy with photonic crystals, the interaction of SPPs with the plasmonic crystal lattice leads to the creation of SPP Bloch modes as the eigenmodes of the crystal. The geometry of the crystal determines the dispersion of these modes, which ultimately governs the propagation of plasmon waves on the nanostructured area as well as their interaction with illuminating light^{11,21–30}. SPPCs have been widely studied, both in the far-field and near-field, however, the vast majority of studies consider either plane wave illumination of the entire crystal, when the whole structure responds in a collective fashion, or their interaction with SPP illumination coming from the unstructured area.

Under collimated illumination, light interaction with plasmonic crystals involves the resonant excitation of the crystal's SPP Bloch modes at frequencies and in directions determined by the overlap with the spectrum of allowed SPP states and the polarisation of the excitation light^{11,21,23}. While such considerations are generally valid only for infinite crystals, the effects of finite size plasmonic crystals is accounted for by considering the effects of

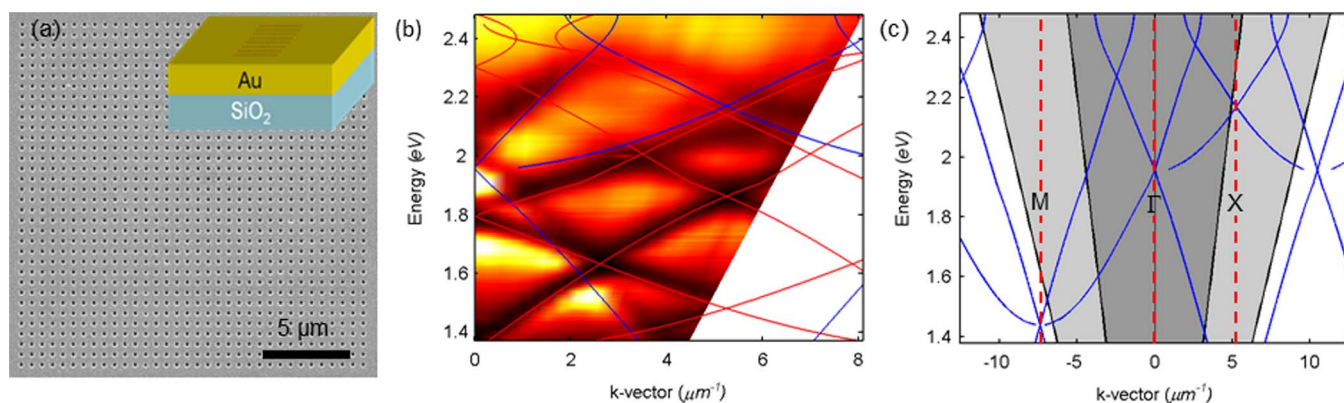


Figure 1 | The plasmonic crystal and its SPP mode structure. (a) Scanning electron microscope (SEM) image of the plasmonic crystal with period 600 nm and hole diameter 200 nm. Inset shows the schematics of the sample geometry. (b) Far-field transmission dispersion of the crystal in (a) measured with p-polarised incident light. The calculated spectrum of Bragg-scattered SPPs, representing the Bloch modes of the crystal, is super-imposed onto the experimental data along with the SPP modes at the Au-air interface (blue) and the Au-glass interface (red). (c) Empty lattice model calculations of the SPP Bloch modes dispersion showing boundaries of the first Brillouin zone of the crystal for the Au-air interface in the Γ -X and the Γ -M directions. The parts of the dispersion corresponding to the range of incident angles accessible with the illumination through the objectives with the NA of 0.45 and 0.9 are shown in dark and light grey, respectively.

the boundary on Bloch mode propagation: at the interface between the nanostructured and unstructured areas, the Bloch modes are refracted, thus allowing for efficient excitation of SPPs onto the smooth metal film surrounding the plasmonic crystal via transmission through the interface^{22,23,29,31}.

However, the focussed illumination of plasmonic crystals differs from the collimated one in three important ways. Firstly, focusing generates a distribution of wavevectors in the incident light beam interacting with the nanostructured area and hence introduces the possibility of simultaneously exciting multiple Bloch modes with different momenta. Secondly, for strongly focussed beams the polarisation in the focal plane has various components not present in the collimated beam. Finally, the number of unit cells illuminated is greatly reduced due to the reduction in the illumination spot size, so that SPPs generated in one part of the crystal are free to propagate through the crystal without interfering with SPPs generated elsewhere, as would be the case were the crystal under plane wave illumination.

In this work, SPP beam excitation inside and outside plasmonic crystals under focussed illumination is investigated experimentally using hyperspectral near-field imaging. The experimental results are rationalised theoretically using a vectorial dipolar model accounting for multiple SPP scattering. The simultaneous excitation and propagation of different order Bloch modes on the nanostructured area and their transmission through the crystal's interface onto the smooth metal film have been studied. The sensitivity of the propagation direction and shape of the plasmonic beams to the illumination conditions were investigated. The results presented in this work open up new opportunities for designing novel SPP launchers providing both beam shape and direction control. Furthermore, this work has strong implications for the design of ultra-fast active plasmonic devices using SPPCs, where the switching and directing of signal SPP beams can be achieved by, e.g., electro-optical, all-optical or electro-mechanical control of the size, position and/or polarisation of the excitation beam.

Results

The effects of focussed illumination on the plasmonic behaviour of SPPCs were investigated on a 2D crystal comprised of circular holes of 200 nm diameter arranged in a square lattice with a periodicity of 600 nm. The overall size of the crystal is approximately $20 \times 20 \mu\text{m}^2$, corresponding to 33 lattice periods (Fig. 1a). The dispersion of the SPP Bloch modes supported by the crystal, as characterized by plane-

wave illumination, exhibits the usual system of allowed and forbidden bands (Fig. 1b, c). The near-field behaviour of the plasmonic crystal under focussed illumination was experimentally probed for two different numerical apertures (NA): 0.45 and 0.9. For both NAs considered in this work, the size of the Gaussian-shaped illumination spot on the plasmonic crystal is about $1 \mu\text{m}$ in diameter (FWHM), therefore only a 2×2 array of holes is illuminated (see Methods).

In contrast to the behaviour of the crystal under collimated (plane wave) illumination, where SPP waves with a width determined by the crystal size are excited (see, e.g., Refs. 15,22,23,29), focussed illumination generates SPP beams of widths much smaller than the size of the crystal and with different propagation directions both inside and outside the crystal (Fig. 2(a-f) and movie M1 for NA = 0.45 and Fig. 3(a-f) and movie M2 for NA = 0.9). For both focusing conditions considered here, SPP beams of reduced spatial widths propagate on the crystal preferentially in both the (1,0) and (0,1) directions for wavelengths exceeding 650 nm. For shorter wavelengths SPP beams propagating in the (1,1) directions are also observed. Increasing the range of wavevectors present in the illumination even further by tighter focusing (Fig. 3) leads to a more complex near-field distribution as the (1,1) Bloch modes are then observed across the entire wavelength range considered. This behaviour is consistent with the calculated dispersion of the crystal (Fig. 1(c)) which indicates that for the range of incident wavevectors corresponding to both illumination conditions, the lattice supports $(\pm 1,0)$ modes, propagating in either the x or y direction throughout the wavelength range under study. However, the wavevector spectrum provided by an NA of 0.45 can only populate the (1,1) modes, propagating at 45° to the lattice principal axes, for wavelengths shorter than 655 nm, whereas the larger range of wavevectors provided by an NA of 0.9, allows for the excitation of these modes across the entire spectral range.

At the crystal boundaries, both the reflection back into the crystal and transmission onto the smooth film of SPP beams can be observed. Using the larger NA of 0.9 enables observation of the strong refraction of the (1,1) modes as they are now populated at frequencies having propagation lengths which are sufficiently long to reach and interact with the crystal boundary. In this case, the $(\pm 1,0)$ modes refract at normal incidence since the crystal boundary is perpendicular to the $(\pm 1,0)$ directions.

Discussion

In order to understand the complex near-field distributions observed experimentally, it is necessary to consider the effects of both the

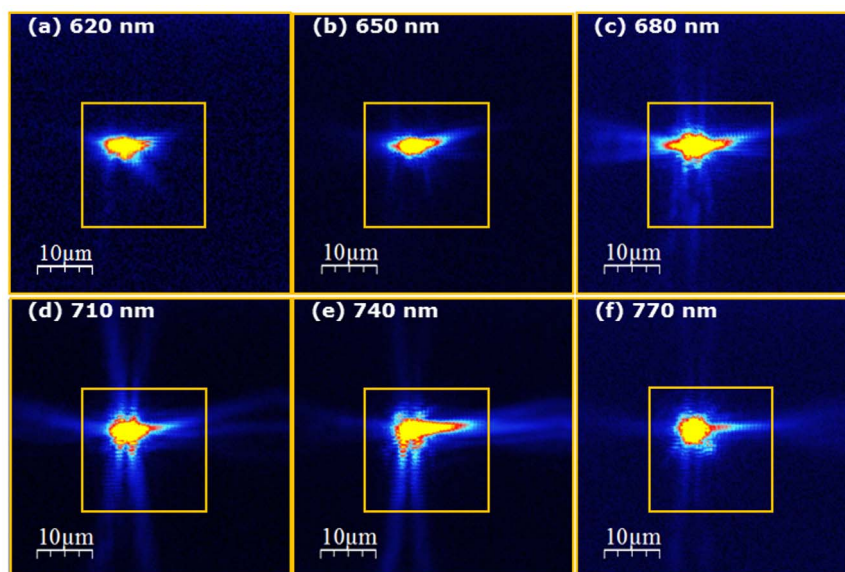


Figure 2 | Near-field optical properties of the finite-size plasmonic crystal under focussed illumination ($NA = 0.45$). (a–f) SNOM images extracted from the movie M1 for focussed illumination ($NA = 0.45$) of the plasmonic crystal for six representative wavelengths. The wavelength is indicated on each frame and the polarisation is horizontal. The nanostructured area is indicated by the square. Due to the difference in intensity, in order to visualise the SPP modes, the contrast has been saturated for the illumination spot. Plasmonic crystal parameters are as in Fig. 1.

reduced illumination area and the focus-driven generation of multiple incident wavevectors on the excitation and propagation of SPP beams in plasmonic crystals.

Effect of local illumination. The focussed illumination spot size ($\sim 1 \mu\text{m}$ FWHM) results in an illuminating area corresponding to a 2×2 array of holes subjected to a Gaussian intensity profile. Under these conditions, the illuminated lattice elements play the role of localised SPP sources effectively acting as an antenna converting incident photons into SPP beams inside the crystal. These beams then propagate across the crystal without interfering with other SPP sources that would be created under plane wave, i.e. global, illumination. The in-plane emission diagram of this antenna defines both the preferential excitation directions and width of the

SPP beams. As a result, the excited SPP Bloch modes of the overall crystal are defined by the overlap, in both frequency and momentum space, of the in-plane scattering diagram of the local antenna and the allowed modes of the crystal governed by the SPP band-diagram, discussed in the following section.

The simulated SPP emission pattern for a 2×2 dipole array excited by a focussed Gaussian beam with the same parameters as in the experiment (Fig. 4) shows that the in-plane scattering diagram, resulting from the interference between the fields emitted by the illuminated dipoles in the antenna, is only weakly dependent on wavelength. A broad SPP beam is excited on each side of the 2×2 array, in the x direction, parallel to the excitation polarisation, while two narrow SPP beams, having lateral dimensions much smaller ($\sim 30 \text{ nm}$ with divergence of $\sim 25^\circ$) than the distance between the

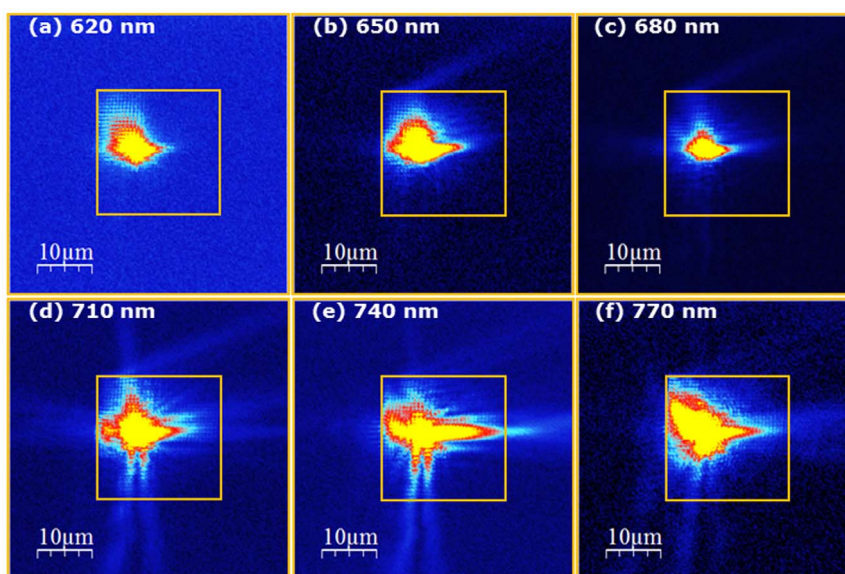


Figure 3 | Near-field optical properties of the finite-size plasmonic crystal under focussed illumination ($NA = 0.9$). (a–f) SNOM images extracted from the movie M2 for focussed illumination ($NA = 0.9$) of the plasmonic crystal for six representative wavelengths. All other parameters and conventions are as in Fig. 2.

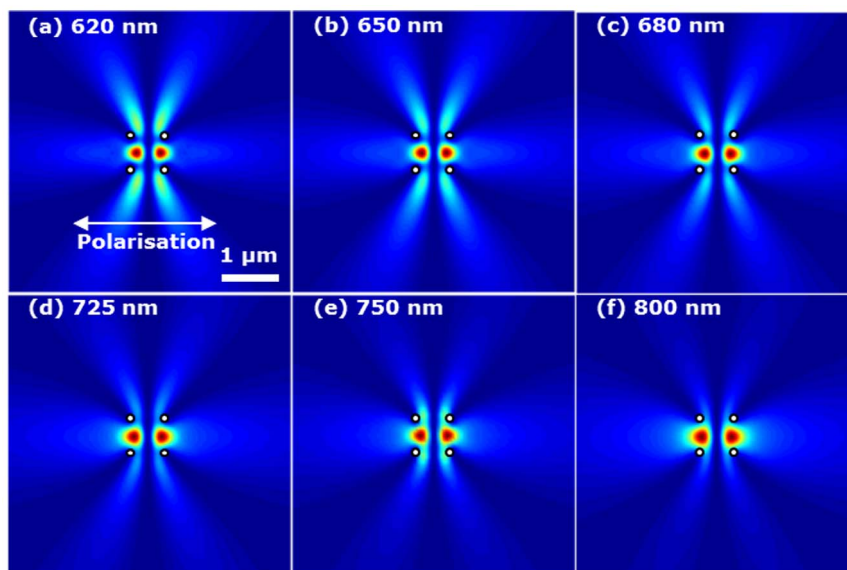


Figure 4 | SPP emission pattern under focussed illumination. Near-field intensity distribution simulated around a 2×2 hole array under focussed illumination for different wavelengths. The array is illuminated by a focussed Gaussian beam with the same parameters as in the experiment ($NA = 0.45$, illumination spot diameter of $1 \mu\text{m}$). The position of the illuminating spot has been chosen to correspond to the experimental conditions and is located in the centre of the 2×2 array.

scatterers, are excited on each side of the array in the orthogonal y direction. It should be noted that the latter plasmonic beams are more pronounced for shorter wavelengths.

Filtering effect. The interaction of the in-plane scattering cross-section of this local SPP source with the optical modes of the crystal lattice results in further filtering of the wavevectors according to the band diagram of the structure, and is at the origin of the SPP beams observed in the experiment. The calculated near-field intensity maps corresponding to different size arrays illuminated locally clearly illustrate this phenomenon (Fig. 5). As the plasmonic beams interact with a larger portion of the periodic potential, the original emission diagram of the localised SPP source evolves into the recognisable (1,0) SPP Bloch modes in both the x and y directions. For the wavelength range investigated in this work, as little as four to six scatterers on each side of the antenna suffice to filter the in-plane emission diagram of the local SPP source into the crystal's SPP Bloch modes.

After filtering by the periodic potential, the distinctive SPP beams observed in the experimental results are recovered, thereby confirming that the origin of the complex near-field behaviour of plasmonic crystals under focussed illumination is determined by the convolution of the scattering diagram of the irradiated antenna and the SPP band diagram of the crystal.

Interaction with the boundary of finite size SPPC. Studying the near field distribution generated when the position of the SPP antenna is offset from the centre of the SPPC facilitates analysis of the different ways in which the antenna's emission can interact with the boundary. This corresponds to a displacement of the illumination from the geometrical centre of the crystal as may occur during an experiment (Figs. 2, 3). First of all, due to the symmetry of the lattice, the propagation of SPPs in the x and y directions is both governed by the band diagram in the Γ - X orientation of the reciprocal lattice. As a result, differences between SPPs propagating in those two directions which are observed in both the experimental results (Figs. 2, 3) and the corresponding calculated near-field intensities (Figs. 6, 7), may be attributed to the emission diagram of the local SPP source.

In the case of the lower NA of 0.45 (Figs. 2, 6), as discussed above, the in-plane SPP scattering cross-section of the 2×2 hole array

shows a single broad beam in the x direction and two narrower beams in the y direction. The larger width of the SPP beams excited in the x direction leads to interactions with a larger portion of the crystal boundary. This results in an SPP interference pattern on the smooth metal film having 2 or 3 maxima for wavelengths ranging from 770–800 nm and 725–750 nm respectively, in close agreement with the experimental results.

However, in the y direction the two beams excited by the local SPP source have a width smaller than the period of 600 nm, resulting in interaction with a reduced portion of the crystal boundary. The only noticeable interaction is a directional broadening of the SPP beams at the boundary of the crystal, before being coupled to SPPs onto the smooth metal film. Furthermore, for wavelengths shorter than 650 nm SPP beams are also coupled in the (1,1) directions in addition to propagating along the (1,0) and (0,1) directions. As mentioned earlier, this behaviour is observed in both the experimental results (Fig. 2(a)) and the calculated field maps (Fig. 6(a)) and is consistent with the calculated Bloch mode spectrum of the nanostructure (Fig. 1(b, c)).

A similar, yet more complex behaviour, is observed in the calculated near-field intensity maps corresponding to illumination with $NA = 0.9$ (Fig. 7). This is due to the population of the (1,1) modes for wavelengths up to 800 nm, as discussed earlier. Refraction of the (1,1) modes by the crystal's interface is observed at smaller angles in the simulations than in the experiment, as the difference in effective index between the nanostructured area and the smooth metal film is underestimated in the model which does not account for the presence of air inside the holes on the nanostructured area.

Controlling SPP beaming. The focussed illumination scheme described here opens up a route for simple and versatile control of SPP excitation by controlling the in-plane scattering diagram of a local SPP source. Being governed by the interference between the various dipoles present in the illuminated area, the response of the local SPP source is strongly dependent on the many illumination parameters: the NA, the illumination spot position, size and polarisation with regards to the antenna. Controlling the illumination NA modifies the polarisation state in the strongly focussed illumination area, thereby influencing the coherent emission of the source. Fig. 8(a,b) shows the emission diagram of a 2×2 dipole array

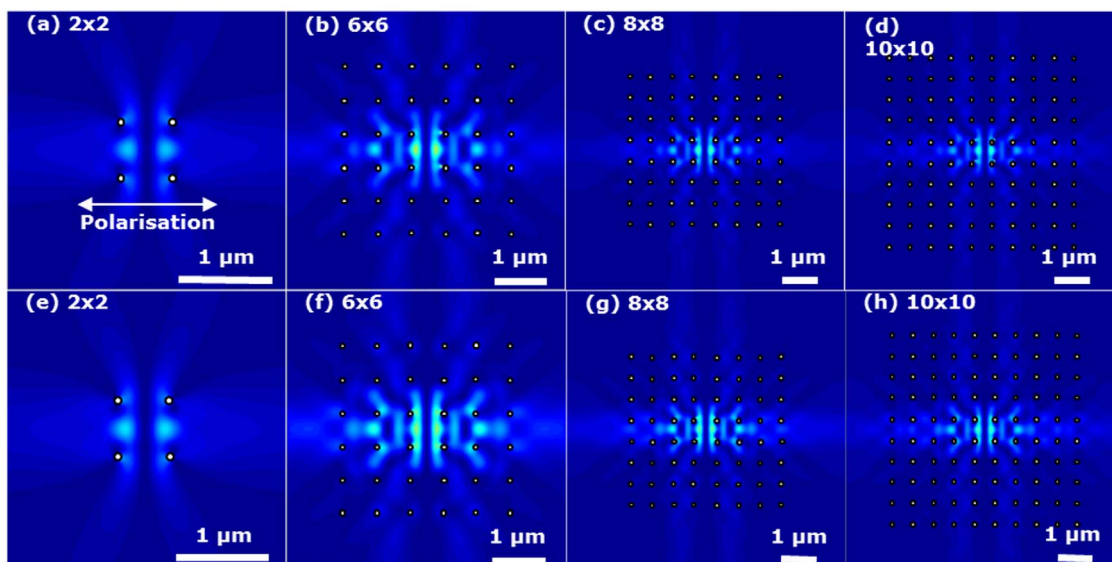


Figure 5 | SPP filtering by the periodic lattice. The simulated SPP emission pattern for 4 different sizes of the nanostructured area illuminated by a focussed beam with the same parameters as in the experiment ($NA = 0.45$, illumination spot of $1 \mu\text{m}$ FWHM) for a wavelength of (a–d) 680 nm and (e–h) 710 nm .

excited by a Gaussian beam corresponding to two different NAs. The in-plane emission in the direction parallel to the incident polarisation is significantly suppressed for the higher NA as in this case the polarisation is no longer preferentially along x .

Alternatively, control over the illumination spot position allows the relative phase of the SPPs excited by each scatterer in the antenna to be adjusted and thus presents the ability to regulate the overall in-plane interference pattern. To illustrate this effect, the emission diagram generated by a further two different geometries were calculated under identical illumination conditions (Fig. 8(c, d)) which yield different SPP emission patterns for each combination of the local SPP source geometry.

From local illumination to collective behaviour. As noted above, due to the reduced number of unit cells driven by the excitation field

in each direction, the 2×2 array of holes responsible for the excitation of SPPs Bloch modes in the crystal does not exhibit the collective behaviour observed when a larger portion of a plasmonic crystal is illuminated. The transition between the local illumination response described above and the well-known collective behaviour of the crystal was investigated at the crystal's resonant wavelength of 620 nm , by calculating the near-field response of a 4×4 array of holes as a function of the illumination spot size, while keeping the NA constant at 0.45 (Fig. 9). As the spot size increases and each of the individual holes within the antenna contributes more equally to the excitation of Bloch modes, the collective behaviour of the plasmonic crystal is recovered, characterised by the typical periodic field distribution on the nanostructured area and the preferential coupling of SPPs onto the smooth metal film in the direction parallel to the incident light polarisation.

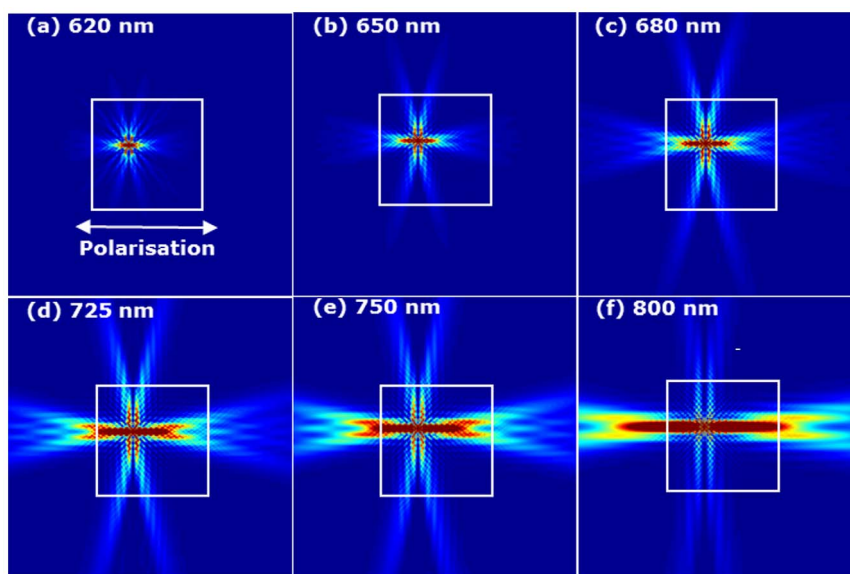


Figure 6 | SPP mode propagation ($NA = 0.45$). (a–f) Near-field intensity distributions simulated for different wavelengths under focussed illumination ($NA = 0.45$) of the plasmonic crystal for six representative wavelengths. The polarisation is horizontal as shown in (a). The nanostructured area is shown by the square. Due to the difference in intensity, in order to visualise the SPP modes, the contrast has been saturated at the illumination spot. The position of the spot centre is located in the centre of the 2×2 array in the centre of the crystal. All other parameters are as in Fig. 1.

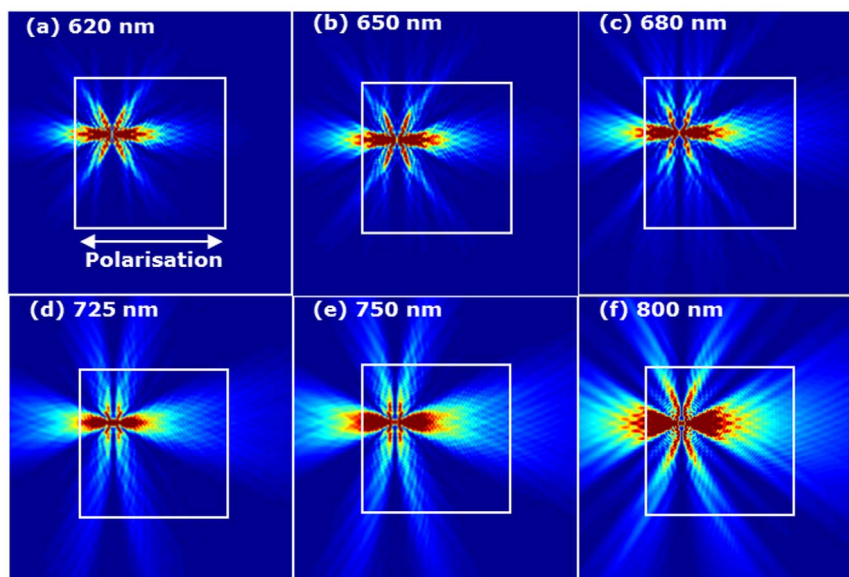


Figure 7 | SPP mode propagation ($NA = 0.9$). (a–f) Near-field intensity distributions simulated for different wavelengths under focussed illumination ($NA = 0.9$) of the plasmonic crystal for six representative wavelengths. All other parameters and conventions as in Fig. 2.

Known edge effects from the collective behaviour of the 4×4 array can be identified (Fig. 9(d–f)) leading to the focusing of the SPPs coupled to the smooth metal film. Furthermore, the range of wavevectors considered here remains sufficiently large (-4.56 to $4.56 \mu\text{m}^{-1}$ for a wavelength of 620 nm) to populate the $(1, +/ - 1)$ SPP modes which are then scattered at the corners of the array. It is worth noting the relatively small array size needed to recover the collective behaviour (4×4); this agrees with the minimum number of scatterers identified earlier for Bloch mode filtering as both phenomena are directly linked to the SPP lifetime on the crystal¹⁶.

In conclusion, this work presents a detailed investigation of the process of plasmonic beam generation using finite size plasmonic crystals under focussed illumination. It was found that the illuminating area acts as a local plasmonic antenna embedded in the periodic structure of the crystal, which conditions its radiation via Bloch mode filtering. This combination of local antenna and plasmonic crystal, allows one to achieve on-demand control of the phase and amplitude of the local plasmonic sources and thus generate, direct and shape plasmonic beams from the crystal onto the surrounding smooth metal film. The combination of illuminating spot size, position, wavelength and polarisation as well as the size of the crystal allows efficient SPP beam shaping and directionality control at normal incidence and switching of SPP beams may be achieved by changing the illumination position or size. Under this excitation scheme, the SPPC serves as a versatile photon-to-SPP conversion device acting as an on-chip SPP source, therefore offering a wide range of functionalities in the fields of integrated plasmonic circuits, demultiplexing devices, routers and sorters, as well as all-optical

interconnections for optical information processing. It will also pave the way to the integration of plasmonic devices with micro- and nano-electromechanical systems (MEMS and NEMS) as well as electro- and all-optical beam steering since both the illumination beam position and polarization can be used to switch and modulate plasmonic waves.

In comparison to the standard plane wave illumination of reduced-size structures, the method described here offers far greater level of control over the excitation and propagation of SPPs while also providing larger design freedom. In particular, control over the SPP mode directionality is obtained by a combination of in-plane scattering diagram of the illuminated scatterers, crystal lattice filtering, and crystal boundary refraction. Proper engineering of the crystal's properties at each of the above steps allows yet additional control over the SPP beams. Using focussed illumination to couple to SPP beams with plasmonic crystals also has the advantage of offering a greater robustness to misalignments, making the proposed solution viable for the production of commercial devices. This approach can be generalised to any kind of surface waves, not necessarily plasmonic, as it can also be used to coupling light in planar dielectric waveguides for data- and tele-communication applications, as well as the generation and control of non-diffractive SPP beams.

Methods

Sample preparation. The plasmonic crystals were fabricated in a 100 nm thick gold film using focussed ion beam (FIB) milling. The gold film was magnetron sputtered onto a glass cover slip using a 10 nm thick Ta_2O_5 adhesion layer. The plasmonic crystals are comprised of circular holes of 200 nm diameter arranged in a square lattice with a period of 600 nm. The overall size of the crystals is $20 \times 20 \mu\text{m}^2$

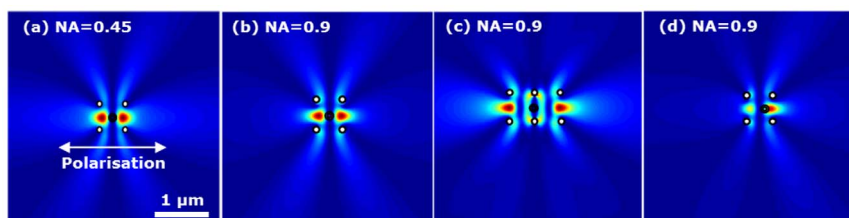


Figure 8 | Control over the SPP emission diagram. SPP emission pattern simulated for a 2×2 hole arrays illuminated by a focussed beam with (a) $NA = 0.45$ and (b–d) $NA = 0.9$ at a wavelength of 725 nm when the beam is incident at different positions indicated by a white circle.

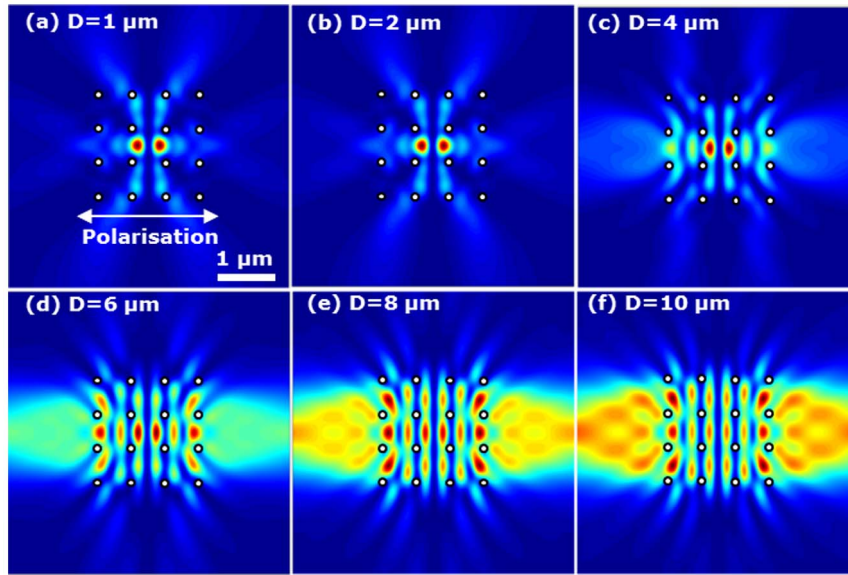


Figure 9 | From local to collective behaviour. Near-field distributions simulated around a 4×4 hole array for a wavelength of 620 nm for focussed illumination (NA = 0.45) of the plasmonic crystal for different spot diameters D.

corresponding to 33 lattice periods (Fig. 1a). The dispersion of SPP Bloch modes supported by the crystal represents usual system of allowed and forbidden bands (Fig. 1b, c).

Near-field spectroscopy. In order to directly visualise the SPP interactions with the plasmonic crystals, a spectroscopic SNOM^{16,22,32} was used, which allows simultaneous imaging of the near-field distribution at all wavelengths between 400 nm and 1000 nm. Coherent broadband light from a supercontinuum laser source was used to illuminate the sample from the substrate side. The light is first injected into a photonic crystal fibre in order to spatially localise all wavelengths in the same Gaussian spot which was then collimated using a microscope objective (NA = 0.2, $f = 22.5$ mm) before being polarised and finally focussed onto the sample through a high NA microscope objective (NA = 0.45, $f = 3.6$ mm, or NA = 0.9, $f = 3.0$ mm). The size of the illuminated area on the sample, defined by the ratio of the focal lengths of the objectives used and the mode extension size in the photonic crystal fibre, is of the order of 1 μm (FWHM) in both cases. The structure was successively illuminated with 2 different microscope objectives and for each illumination scheme, the near-field images were recorded to allow for comparison.

The signal collected by the SNOM probe is spectrally separated by a spectrometer coupled to a CCD camera, allowing acquisition of the full near-field spectrum at each pixel of the SNOM image. The probes used are pulled optical fibres coated with a 250 nm gold layer. A nano-aperture with a typical size of the order of 50 nm is created using focussed ion beam milling at the tip of the fibre. It should be noted that, based on a comparison with the numerical simulations, the SNOM probe can be considered as passive, meaning that its scattering does not contribute to the excitation of SPPs.

Numerical modelling. The coupling to and scattering of SPPs by the crystal lattice have been theoretically investigated using a point-dipole model allowing for rapid and accurate calculation of the near-field distributions on both the nanostructured and unstructured areas of the metal film.

The point dipole model used here has been proven accurate in the simulation of SPP microcomponents and photonic band gap structures formed by a set of dipolar nano-particles^{33,34}. The model exploits the analytic representation of the Green dyadic describing the scattering via SPP excitation. Following this description, the self-consistent field at the site of the scatterers in the process of multiple scattering takes the form

$$E(r_j) = E_0(r_j) + k_0^2 \sum_{j \neq i} G(r_i, r_j) \cdot \alpha \cdot E(r_j), \quad (1)$$

where $E_0(r_j)$ is the self-consistent field at the site of scatterer i , k_0 is the wave vector of the incoming field in space, $G(r_i, r_j)$ is the Green tensor for near and far field regions, also known as the total field propagator, α is the polarisability of the scatterers, and $E(r_j)$ is the field at the site of scatterer j . Here, the polarisability α has the surface dressing included i.e. the coupling of the dipole to itself through reflection in the surface. Furthermore, the polarisability, α , is a tensor, describing the polarisability in each direction:

$$\alpha = \left(I - k_0^2 \frac{\alpha^0}{\epsilon_0} \cdot G^s(r, r') \right)^{-1} \cdot \alpha^0, \quad (2)$$

where α^0 is the free space polarisability tensor given as

$$\alpha^0 = \epsilon_0 I 4\pi a^3 \frac{\epsilon - 1}{\epsilon + 2}, \quad (3)$$

with I being the unit dyadic tensor, ϵ is the wavelength dependent dielectric function of the metal, a is the radius of one scattering element, and ϵ_0 is the vacuum permittivity. Note that equation (2) is valid under the long-wavelength electrostatic approximation which assumes that the field is constant within the considered range, corresponding in the present case to the size of one scatterer. Therefore, for the approximation to be valid, the wavelength must be much larger than the size of the scatterers considered. Applying the image dipole approximation to $G^s(r, r')$ in Eq. (2), the following result is obtained for the polarisability tensor of Eq. (1).

$$\alpha \approx \left[I - \frac{\epsilon_2 - 1}{\epsilon_2 + 1} \cdot \frac{\epsilon_2 - 1}{\epsilon_2 + 2} \left(\frac{1}{8} \hat{x}\hat{x} + \frac{1}{8} \hat{y}\hat{y} + \frac{1}{4} \hat{z}\hat{z} \right) \right]^{-1} \cdot \alpha^0. \quad (4)$$

When Eq. (4) has been used in Eq. (1) to determine the polarisation, the final step is to calculate the field outside the scatterer as a self-consistent field:

$$E(r) = E^0(r) + k_0^2 \sum_i^N G(r, r_i) \cdot \alpha \cdot E(r_i). \quad (5)$$

The Green tensor for SPP-to-SPP scattering is the sum of a direct contribution, G^d , in this case the free space Green's tensor, and an indirect contribution, G^s , describing both reflection from the metal/dielectric interface and SPP excitation. Considering both the source and observation points being close to a metal surface but far away from each other, one can propose the use of a three-dimensional dyadic Green's tensor approximation which only accounts for the SPP elastic scattering channel and which includes both direct and indirect terms. Therefore, the Green dyadic can be represented by

$$G_{SPP}(r, r') \approx a_{zz}(\lambda) \exp[ik_z(z+h)] H_0^1(k_\rho \rho) \times \left[\hat{z}\hat{z} + (\hat{z}\hat{\rho} - \hat{\rho}\hat{z}) \frac{k_z}{k_\rho} - \hat{\rho}\hat{\rho} \left(\frac{k_z}{k_\rho} \right)^2 \right], \quad (6)$$

where H_0^1 is the zero-order Hankel function of the first kind, $\rho = |r_{\parallel} - r'_{\parallel}|$, $\hat{\rho} = \frac{(|r_{\parallel} - r'_{\parallel}|)}{\rho}$, with \parallel referring to the projection of the radius vector on the xy plane which coincides with the metal/air interface, and z refers to the height of the observation point r above the surface, while h refers to the height of the source point r' . Finally, κ_ρ and κ_z are the components of the three-dimensional SPP wave vector



$$\kappa_{\rho} = k_0 \sqrt{\frac{\varepsilon}{\varepsilon + 1}}, \quad \kappa_z = \sqrt{k_0^2 - \kappa_{\rho}^2}, \quad (7)$$

and

$$a_{zz}(\lambda) = \frac{\kappa_{\rho}}{2} \left[\sqrt{\varepsilon} \left(1 - \frac{1}{\varepsilon^2} \right) \frac{1 + \varepsilon}{\varepsilon} \right]^{-1}. \quad (8)$$

The Green dyadic described above has proven effective in analysing plasmonic phenomena in a variety of contexts³⁵. Here we consider the response of a plasmonic crystal of N holes when illuminate by a focussed Gaussian beam. The incident beam is assumed to be a fundamental Gaussian beam before the lens and polarized in the x direction to match the experimental conditions. The holes are treated as point scatterers on the surface of the metal film, a reasonable approximation considering the assumed sub-wavelength size of the holes.

- Siviloglou, G. A. & Christodoulides, D. N. Accelerating finite energy Airy beams. *Opt. Lett.* **32**, 979–81 (2007).
- Lin, J. *et al.* Cosine-Gauss Plasmon Beam: A Localized Long-Range Nondiffracting Surface Wave. *Phys. Rev. Lett.* **109**, 093904 (2012).
- Minovich, A. *et al.* Generation and Near-Field Imaging of Airy Surface Plasmons. *Phys. Rev. Lett.* **107**, 116802 (2011).
- Wang, F., Yang, J., Chen, L., Jiang, X. & Wang, M. Optical switch based on multimode interference coupler. *IEEE Photonics Technol. Lett.* **18**, 421–423 (2006).
- Kalavrouziotis, D. *et al.* Demonstration of a Plasmonic MMI Switch in 10-Gb/s True Data Traffic Conditions. *IEEE Photonics Technol. Lett.* **24**, 2012 (2012).
- Le Guyader, L. *et al.* Coherent control of surface plasmon polariton mediated optical transmission. *J. Phys. D: Appl. Phys.* **41**, 195102 (2008).
- Aieta, F. *et al.* Aberration-free ultrathin flat lenses and axicons at telecom wavelengths based on plasmonic metasurfaces. *Nano Lett.* **12**, 4932–6 (2012).
- Ni, X., Emani, N. K., Kildishev, A. V., Boltasseva, A. & Shalaev, V. M. Broadband light bending with plasmonic nanoantennas. *Science* **335**, 427 (2012).
- Chen, W. T. *et al.* High-efficiency broadband meta-hologram with polarization-controlled dual images. *Nano Lett.* **14**, 225–30 (2014).
- Ni, X., Kildishev, A. V. & Shalaev, V. M. Metasurface holograms for visible light. *Nat. Commun.* **4**, 2807 (2013).
- Zayats, A. V., Smolyaninov, I. I. & Maradudin, A. A. Nano-optics of surface plasmon polaritons. *Phys. Rep.* **408**, 131–314 (2005).
- Kitson, S. C., Barnes, W. L. & Sambles, J. R. Full Photonic Band Gap for Surface Modes in the Visible. *Phys. Rev. Lett.* **77**, 2670–2673 (1996).
- Krenn, J. R., Wolf, R., Leitner, A. & Aussenegg, F. R. Near-field optical imaging the surface plasmon fields of lithographically designed nanostructures. *Opt. Commun.* **137**, 46–50 (1997).
- Bozhevolnyi, S. I., Vohnsen, B., Smolyaninov, I. I. & Zayats, A. V. Direct observation of surface polariton localization caused by surface roughness. *Opt. Commun.* **117**, 417–423 (1995).
- Garcia-Ortiz, C. E., Coello, V., Han, Z. & Bozhevolnyi, S. I. Generation of diffraction-free plasmonic beams with one-dimensional Bessel profiles. *Opt. Lett.* **38**, 905–7 (2013).
- Bouillard, J.-S., Vilain, S., Dickson, W., Wurtz, G. A. & Zayats, A. V. Broadband and broadangle SPP antennas based on plasmonic crystals with linear chirp. *Sci. Rep.* **2**, 829 (2012).
- Benetou, M. I., Thomsen, B. C., Bayvel, P., Bouillard, J.-S., Dickson, W. & Zayats, A. V. “Visualization of high-order plasmonic Bloch modes in square-lattice plasmonic crystals”, SPP5 - The Fifth International Conference on Surface Plasmon Photonics, Busan, Korea (15 May–20 May 2011).
- Shegai, T. *et al.* A bimetallic nanoantenna for directional colour routing. *Nat. Commun.* **2**, 481 (2011).
- Liu, J. S. Q., Pala, R. A., Afshinmanesh, F., Cai, W. & Brongersma, M. L. A submicron plasmonic dichroic splitter. *Nat. Commun.* **2**, 525 (2011).
- Baron, A. *et al.* Compact antenna for efficient and unidirectional launching and decoupling of surface plasmons. *Nano Lett.* **11**, 4207–4212 (2011).
- Dickson, W., Wurtz, G. A., Evans, P. R., Pollard, R. J. & Zayats, A. V. Electronically controlled surface plasmon dispersion and optical transmission through metallic hole arrays using liquid crystal. *Nano Lett.* **8**, 281–286 (2008).

- Bouillard, J.-S., Vilain, S., Dickson, W. & Zayats, A. V. Hyperspectral imaging with scanning near-field optical microscopy: applications in plasmonics. *Opt. Express* **18**, 16513–16519 (2010).
- Mikhailov, V., Wurtz, G., Elliott, J., Bayvel, P. & Zayats, A. V. Dispersing light with surface plasmon polaritonic crystals. *Phys. Rev. Lett.* **99**, 083901 (2007).
- Benetou, M. I., Thomsen, B. C., Bayvel, P., Dickson, W. & Zayats, A. V. Four-level polarization discriminator based on a surface plasmon polaritonic crystal. *Appl. Phys. Lett.* **98**, 111109 (2011).
- Bouillard, J.-S. *et al.* Optical transmission of periodic annular apertures in metal film on high-refractive index substrate: The role of the nanopillar shape. *Appl. Phys. Lett.* **96**, 201101 (2010).
- Drezet, A. *et al.* Opening the light extraction cone of high index substrates with plasmonic gratings: Light emitting diode applications. *Appl. Phys. Lett.* **95**, 021101 (2009).
- Ding, B., Hrelescu, C., Arnold, N., Isic, G. & Klar, T. A. Spectral and directional reshaping of fluorescence in large area self-assembled plasmonic-photonics crystals. *Nano Lett.* **13**, 378–86 (2013).
- Bouillard, J.-S. G., Dickson, W., O'Connor, D. P., Wurtz, G. A. & Zayats, A. Low-temperature plasmonics of metallic nanostructures. *Nano Lett.* **12**, 1561–1565 (2012).
- Genet, C. & Ebbesen, T. W. Surface Plasmon Mode Steering and Negative Refraction. *Phys. Rev. Lett.* **266804**, 4 (2010).
- McCarron, R., O'Connor, D., Bouillard, J.-S., Dickson, W. & Zayats, A. V. Light extraction beyond total internal reflection using one-dimensional plasmonic crystals. *Appl. Phys. Lett.* **99**, 081106 (2011).
- Dolev, I., Epstein, I. & Arie, A. Surface-Plasmon Holographic Beam Shaping. *Phys. Rev. Lett.* **109**, 203903 (2012).
- Bouillard, J.-S. G., Dickson, W., Wurtz, G. A. & Zayats, A. V. Near-Field Hyperspectral Optical Imaging. *ChemPhysChem* **15**, 619–629 (2014).
- Bozhevolnyi, S. I. & Volkov, V. S. Multiple-scattering dipole approach to modeling of surface plasmon polariton band gap structures. *Opt. Commun.* **198**, 241–245 (2001).
- Segovia, P., Cortes, R., Garcia, C., Elizondo, N. & Coello, V. Coupling of surface-plasmon-polariton in nano-arrays of particles. *J. Opt. Res.* **12**, 4 (2011).
- Segovia, P. & Coello, V. Elastic Surface Plasmon Polariton Scattering: Near- and Far-Field Interactions. *Nano* **07**, 1150003 (2012).

Acknowledgments

This work has been supported, in part, by EPSRC (UK) and the EC FP7 project PLAISIR. A.Z. acknowledges support from the Royal Society and the Wolfson Foundation. P.S.O. is grateful for the support from CONACYT. G.W. is grateful for support from the People Programme (Marie Curie Actions) of the EC FP7 project 304179.

Author contributions

G.W. proposed the work. J.S.B. and W.D. conceived and designed the experiment. J.S.B. performed the experiments. P.S.O. performed the numerical simulations. A.Z., G.W., W.D., J.S.B. and P.S.O. discussed the results and wrote the manuscript.

Additional information

Supplementary information accompanies this paper at <http://www.nature.com/scientificreports>

Competing financial interests: The authors declare no competing financial interests.

How to cite this article: Bouillard, J.-S., Segovia, P., Dickson, W., Wurtz, G.A. & Zayats, A.V. Shaping plasmon beams via the controlled illumination of finite-size plasmonic crystals. *Sci. Rep.* **4**, 7234; DOI:10.1038/srep07234 (2014).



This work is licensed under a Creative Commons Attribution-NonCommercial-NoDerivs 4.0 International License. The images or other third party material in this article are included in the article's Creative Commons license, unless indicated otherwise in the credit line; if the material is not included under the Creative Commons license, users will need to obtain permission from the license holder in order to reproduce the material. To view a copy of this license, visit <http://creativecommons.org/licenses/by-nc-nd/4.0/>